New Journal and we have not received input yet 32 (2022) 101309

Contents lists available at ScienceDirect

Thermal Science and Engineering Progress

journal homepage: www.sciencedirect.com/journal/thermal-science-and-engineering-progress

Production and characterization of novel EPDM/NBR panels with paraffin for potential thermal energy storage applications

Francesco Valentini [a,*], Andrea Dorigato [a], Luca Fambri [a], Massimo Bersani [b], Maurizio Grigiante [c], Alessandro Pegoretti [a,*]

[a] University of Trento, Department of Industrial Engineering and INSTM Research Unit, Via Sommarive 9, 38123 Trento, Italy
[b] Centre for Materials and Microsystems, Fondazione Bruno Kessler, Via Sommarive 18, 38123 Trento, Italy
[c] University of Trento, Department of Civil, Environmental and Mechanical Engineering, Via Mesiano, 77 38123 Trento, Italy

ARTICLE INFO

Keywords:
EPDM
NBR
Thermal energy storage
Phase change materials
Paraffin
Buildings

ABSTRACT

Innovative panels suitable for the thermal management of closed systems with potential applications for buildings have been produced combining an Ethylene-Propylene Diene Monomer (EPDM) rubber with a paraffin wax having a melting temperature of 28 °C. The compounded material was confined in a Nitrile Butadiene Rubber (NBR) envelope that impeded any paraffin leakage. According to differential scanning calorimetry, the effective thermal energy efficiency of the PCM (PCM_{eff}) in the panel, was 37 wt% with a melting enthalpy of about 100 J/g. The homogeneous distribution of paraffin within the elastomeric matrix was verified both through scanning electron microscopy and through temperature monitoring of the panel's surface during heating/cooling cycles, performed by an infrared camera. It was also observed that the thermal conductivity of the panels was the same above or below the melting point of paraffin with values of about 0.15 W/m·K. Shore A hardness tests revealed the dependence on the temperature due to the presence of paraffin that acted as softener above its melting point and as hardener below. The evaluation of the thermal energy storage performance of the panels was verified by monitoring the internal temperature of testing boxes (310x310x310 mm^3) insulated with these elastomeric panels during heating/cooling cycles performed in a temperature interval from 16 to 31 °C (typical summer conditions in Trento, Italy). The presence of paraffin within the elastomeric panels allowed to keep the internal temperature of the box always lower than 27 °C, with a delay of the peak temperature of about 1 h with respect to a reference non-insulated box. The results of testing boxes have been confirmed after 15 months, showing the reproducibility and the stability of the assembled lab configuration.

1. Introduction

Nowadays, due to the concerns related to global warming and to climate change, it is essential to find an equilibrium between the available energy resources and the energy demand [1]. Climate change refers to a persistent variation or variability in the climate, occurring in natural processes, able to change the composition of the atmosphere [2]. In the last century the global primary energy consumption and the CO_2 emissions increased of 10 times [3]. Moreover, the improvement of the living conditions in many countries around the world requires high energy amounts with a consequent more difficult transition to award decarbonization [3,4]. Despite the strong efforts to reduce the CO_2 emissions, in the European Union (EU) in 2018 renewable energy resources contributed only to 18 % of the gross energy productions with a reduction of the greenhouse gases (GHG) emission of around 23 % with respect to 1990 [5–7]. In order to reach the 2050 target (-90 % GHG emissions with respect to 1990), the EU annual reduction of GHG emissions should be around 114–157 Mt CO_2eq, much higher with respect to the annual average reduction between 1990 and 2017 that was around 46 Mt CO_2eq [8,9].

The use of technologies and systems able to store thermal energy allow the accumulation of energy when available (i.e. thermal energy from sun) in order to use it when and where necessary, with a global energy savings and consequent reduction of CO_2 emissions[10–13]. This technology, called thermal energy storage (TES), gives the possibility to balance the energy demand of buildings, reducing the energy absorption peaks for air conditioning in the summer thanks to the presence of TES materials in the building's envelope [14–17]. Generally, TES systems are

* Corresponding authors.
E-mail addresses: francesco.valentini@unitn.it (F. Valentini), alessandro.pegoretti@unitn.it (A. Pegoretti).

https://doi.org/10.1016/j.tsep.2022.101309
Received 18 January 2022; Received in revised form 13 April 2022; Accepted 18 April 2022
Available online 21 April 2022
2451-9049/© 2022 Elsevier Ltd. All rights reserved.

based on the heat absorption/release, during the phase transition of particular materials, that occurs at constant temperature and provides high energy storage capability. These materials are called phase change materials (PCMs) and paraffins are the most widely used thanks to their broad range of melting temperatures, high melting enthalpies, low price and chemical stability [11,18–21]. The main problem is their leakage in the molten state which requires the encapsulation and/or the shape stabilization of the PCM within polymer matrices [22–33] or ceramic structures [34]. Paraffinic PCMs are used for several application, among which thermoregulated building materials [20,35–41], solar energy storage devices [42], sport equipment [43] and smart fabrics [44–46].

Ethylene-Propylene Diene Monomer (EPDM) rubber is one of the most widely used synthetic elastomers thanks to its good mechanical properties, high resistance to ageing, ozone, UV and weathering. It is therefore used for the production of gaskets, O-rings, window profiles, belts and waterproofing membranes. The main disadvantage of EPDM rubber is related to the limited resistance to hydrocarbons, such as oils, kerosene, aromatic compounds, gasoline and halogenated solvents [47]. On the contrary, Nitrile Butadiene Rubber (NBR), is highly resistant to swelling in oils and solvents, but it has poor resistance to ozone and heat aging [48–50]. NBR rubber is used in the automotive industry for the production of O-rings, seals and fuel hoses [51,52].

In the literature, only few works can be found on the thermal energy storage properties of EPDM matrices filled with different kinds of PCMs, and they are mainly focused on the use of paraffin waxes within EPDM foams [37,38] directly mixed within the EPDM matrix in limited quantities to avoid paraffin leakage [21,22] or stabilized with expanded graphite [53]. Despite the possible advantages of using EPDM/NBR/paraffin panels for the thermal energy storage of buildings and the recent European requirements for the energy efficiency of buildings, no studies can be found in the open literature on these systems. Based on these considerations, this work aims to develop EPDM/NBR panels with a high amount of paraffin wax in order to evaluate their performances for the first time, and to verify their possible use for the thermal management of buildings. After a comprehensive microstructural characterization of the prepared materials, the thermo-mechanical properties of the panels were evaluated, with particular attention to the evaluation of the PCM leakage issues and to the TES performances.

2. Experimental part

2.1. Materials

Vistalon® 2504 EPDM rubber, an amorphous terpolymer with low Mooney viscosity (ML 1 + 4, 125 °C), a medium diene content (4.7 wt% of ethylidene norbornene), a low ethylene content (58 wt%) was purchased from Exxon mobil (Irving, TX, USA). Rubitherm® RT28HC, a paraffinic wax with a melting temperature of around 28 °C and a specific melting enthalpy (ΔH_m) of 250 J/g was purchased from Rubitherm® GmbH (Berlin, Germany). This PCM was selected to store/release thermal energy in a temperature interval suitable for building applications, i.e. slightly above room temperature. Zinc oxide (curing activator), stearic acid (curing activator and lubricating agent) and sulphur (vulcanizing agent) were purchased from Rhein Chemie (Cologne, Germany). As accelerators were used tetramethylthiuram disulphide (TMTD) and zinc dibutyl dithiocarbamate (ZDBC), purchased from Vibiplast srl (Castano Primo (MI), Italy). Carbon black N550, purchased from the Omsk Carbon group (Omsk, Russia) was used as reinforcing filler. The composition of the elastomeric compound used for the preparation of the samples in this work is reported in Table 1, and the quantities are expressed in phr. Organophilic montmorillonite Cloisite® 20 was obtained from BYK-Chemie GmbH (Wesel, Germany). NBR (nitrile-butadiene rubber) foils (thickness equal to 0.4 mm), with high acrylonitrile content (45 %) were purchased on the market.

Table 1
Composition of the elastomeric EPDM compound used for the preparation of the composites.

Material	Quantity [phr]
Vistalon® 2504	100
sulphur	3
zinc oxide	3
stearic acid	1
carbon black	20
TMTD	0.87
ZDBC	2.5

2.2. Samples preparation

In order to stabilize the PCM through nanoclay intercalation, the liquid paraffin wax was firstly mixed with the Cloisite® 20 clay (at a constant paraffin/clay ratio of 3:1 [54]) and ultrasonicated for 5 min at 30 °C using a Hielscher UP400S device (Teltow, Germany), equipped with a cylindrical sonotrode with a diameter of 15 mm and operating at a power of 400 W.

EPDM/paraffin blends with a paraffin content of 56 wt% were prepared by melt compounding in an internal mixer (Thermo Haake Rheomix® 600), equipped with counter rotating rotors. The compounding temperature was set at 40 °C and the rotor speed at 50 rpm.

EPDM was firstly added into the mixer with the carbon black and mixed for 5 min, then sulphur, zinc oxide, stearic acid and the accelerators were added and mixed for other 5 min. Paraffin/clay mixture was then gradually added and mixed for 30 min, for a total mixing duration of 40 min. The compound was then transferred in a mould covered with a layer of NBR rubber (ENV), applied to both sides of the EPDM compound to seal it in the inner part. The resulting compound was then vulcanized under a hydraulic press at 170 °C, keeping pressure of 2 bar for 20 min. In this way, square panels of around 110x110x5 mm^3 were obtained.

The list of the prepared samples along with their codes is reported in Table 2. The amount of paraffin Rubitherm® RT28HC and of Cloisite® 20 reported in Table 2 (wt%, phr) were calculated with respect to the total mass of the EPDM/paraffin/clay compound (EPDM + RT28) and not considering the mass of the NBR envelope (ENV). In Fig. 1 a picture of the EPDM + RT28 + ENV sample is shown.

The sample named "EPDM" refers to the neat EPDM rubber.

In order to test the thermal energy storage capability of the produced materials, testing boxes (310x310x310 mm^3) made of wood panels 5 mm in thickness and internally insulated with rubber panels (EPDM or EPDM + RT28 + ENV) with dimensions of around 300x300x5 mm^3, were prepared. In Fig. 2 (a, b) the external and internal side of the wood boxes are shown.

2.3. Experimental methodologies

The Mooney viscosity of the EPDM and EPDM + RT28 samples was measured using a Mooney 1500S viscometer equipped with a ML-type rotor, operating at a temperature of 100 °C for 4 min. The minimum

Table 2
Composition and code of the prepared samples.

Sample code	Vistalon® 2504 [g]	RT28HC [wt% - phr]	Cloisite® 20 [wt% - phr]	NBR rubber envelope [g]	Total mass (without envelope) [g]
EPDM	45.0	–	–	–	59
EPDM + RT28	11.0	56.8–263	15.1–70	–	51
EPDM + RT28 + ENV	10.3	56.8–263	15.1–70	18	47

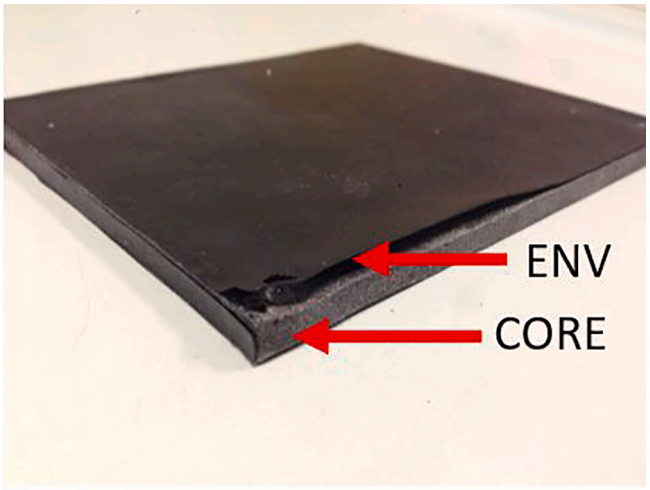

Fig. 1. picture of the EPDM + RT28 + ENV sample.

torque (ML) and the final viscosity after 4 min, ML(1 + 4), were evaluated.

The Mooney scorch time of the EPDM and EPDM + RT28 samples was determined through a Mooney 1500S viscometer equipped with a MS-type rotor, at a temperature of 130 °C for 30 min. The minimum torque (ML), the Mooney scorch time (t_5), defined as the time required to reach a viscosity 5 units above the ML (t_5) and the time required to reach a viscosity 35 units above the ML (t_{35}) were evaluated.

The vulcanization kinetics of the EPDM and EPDM + RT28 samples was investigated by using a Monsanto Rheometer ODR, operating at a temperature of 184 °C for 20 min. The maximum torque (MH), the minimum torque (ML), the time required to reach 90% of MH (t_{90}) and the time required to increase the torque of 2 units above the ML (t_{s2}) were evaluated.

The ability of the external envelope to avoid paraffin leakage was evaluated on the EPDM + RT28 + ENV sample according to two test sequences. In the first sequence two specimens were tested for 24 days performing around 330 heating/cooling cycles between 5 and 40 °C by using a climatic chamber (model DM340C by Angelantoni Industrie Srl, Perugia, Italia). The duration of each cycle was 105 min and the specimens were hung off in order to avoid contact with any surface. In the second sequence the specimens tested in sequence 1, were stored for 2 months in a ventilated oven at around 43 °C. The weight was measured before and after each test, and the residual PCM amount was determined.

The fracture surfaces of the composites were observed through a Vega3 Tescan scanning electron microscope (SEM), operating at an acceleration voltage of 10 kV and equipped with a secondary electron (SE) detector. The samples were prepared cutting 400 μm thick slices, using a Thermo Scientific HM525 NX cryo-microtome at a temperature of −35 °C, with an angle of 10°.

The geometrical density (ρ_{geom}) was calculated on samples with dimensions of 110*110*5 mm^3 measuring the mass through a Gibertini E42 balance (sensitivity of 0.1 mg) and the linear dimensions (and hence the volume) with a caliper (sensitivity of 0.01 mm).

Thermogravimetric analysis (TGA) was performed on neat EPDM, on neat paraffin, on EPDM + RT28, on EPDM + RT28 + ENV and on the NBR envelope (ENV), through a TA Q5000 IR thermobalance under an air-flow of 10 ml/min in a temperature range between 30 and 700 °C, at a heating rate of 10 °C/min. The temperature associated to a mass loss of 5 % ($T_{5\%}$) and the temperatures associated to the maximum degradation rate of the constituents (T_{peak1}, T_{peak2}, T_{peak3}) and the residual mass at 700 °C (m_{700}) were determined.

Differential scanning calorimetry (DSC) measurements were performed on neat paraffin, on EPDM + RT28, and on EPDM + RT28 + ENV, by using a Mettler DSC30 calorimeter under a nitrogen flow of 10 ml/min and at a heating/cooling rate of ± 1 °C/min, as suggested in the literature [37]. A first heating scan from 0 to 40 °C was followed by a cooling scan from 40 to 0 °C and by a second heating scan from 0 to 40 °C. In this way, the melting temperature during the first (T_{m1}) and the second heating scan (T_{m2}), the crystallization temperature (T_c) and the specific melting and crystallization enthalpy values (ΔH_{m1}, ΔH_c, ΔH_{m2}) were obtained. The volumetric specific enthalpy P was evaluated by multiplying the melting and crystallization enthalpy values by the geometrical density, i.e. as $P_{Heat} = \Delta H_m{}^*\rho_{geom}$ and $P_{Cool} = \Delta H_c{}^*\rho_{geom}$, respectively. In the case of paraffin, the density values reported in technical data sheet have been used (0.88 g/cm^3 at the solid state, 0.77 g/cm^3 at the liquid state). The effective PCM content of each sample was determined in the first heating scan (PCM_{m1}^{eff}), in the cooling scan (PCM_c^{eff}) and in the second heating scan (PCM_{m2}^{eff}) as the ratio between the specific enthalpy of the samples and the corresponding specific enthalpy values of the neat paraffin, as shown in Equations (1–3):

$$PCM_{m1}^{eff} = \left(\frac{\Delta H_{m1}}{\Delta H_{m1PCM}}\right)*100 \quad (1)$$

$$PCM_{c}^{eff} = \left(\frac{\Delta H_{c}}{\Delta H_{cPCM}}\right)*100 \quad (2)$$

$$PCM_{m2}^{eff} = \left(\frac{\Delta H_{m2}}{\Delta H_{m2PCM}}\right)*100 \quad (3)$$

a b

Fig. 2. Representative picture of the boxes used for the test: external side (a) and internal side (b).

where ΔH_{m1PCM}, ΔH_{cPCM} and ΔH_{m2PCM} are, respectively, the specific enthalpy values associated to the melting during the first heating scan, crystallization and melting during the second heating scan of the neat PCM.

Shore A hardness was measured using a Hilderbrand Durometer according to the ASTMD2240 standard. Square specimens (70x70x5 mm^3) were tested, after pressing the indenter against the specimen for a time equal to 5 s. The hardness was measured at temperature above (T = 40 °C) and below (T = 0 °C) the melting point of paraffin. At least 30 measurements were performed for each sample.

Compressive properties were measured under quasi-static conditions on squared plates 110 mm wide and 5 mm thick, through an Instron 5969 universal testing machine equipped with a load cell of 10 kN and operating at a crosshead speed of 0.5 mm/min. The tests were performed below (T = 10 °C) and above (T = 40 °C) the melting point of paraffin and the samples were conditioned overnight at the testing temperature before the test. The compressive modulus was measured as a secant value between the strain levels of 0.05 and 0.1 mm/mm for EPDM samples, between 0.1 and 0.15 mm/mm for EPDM + RT28 + ENV samples. The deformation of the samples corresponding to a stress equal to 0.1 MPa ($\varepsilon_{0.1}$) and the stress corresponding to a deformation of 0.1 mm/mm ($\sigma_{0.1}$) have been calculated. At least three specimens were tested for each composition.

Thermal conductivity measurements were carried out using a Neztsch HFM 446 heat flow meter according to ISO 8301 standard. The tests were carried out on squared specimens with dimensions 110 × 110 × 5 mm^3 at a temperature of 10 °C, 30 °C and 40 °C applying a temperature difference of 20 °C between the cold and hot plate of the instrument. The three temperature values were chosen in order to perform the test below (10 °C), across (30 °C) and above (40 °C) the melting point of paraffin. At least three specimens were tested for each sample. Thermal conductivity tests were carried out also according to ISO-22007 standard, on squared specimens with dimensions equal to 110 × 110 × 5 mm^3 using a Hot Disk thermal analyser equipped with a 5465 sensor (diameter of around 6.4 mm). The test was performed at a temperature of 22 °C, applying a power of 60 mW for 40 s in the case of EPDM + RT28 + ENV sample and a power of 30 mW in the case of the EPDM sample. These operating parameters were chosen in order to guarantee a temperature increase of each specimen of at least 2 °C, as reported in the standard. At least five measurements were performed for each sample.

In order to test the thermal energy storage capability of the EPDM + RT28 + ENV sample, boxes with different internal insulation were subjected to heating/cooling cycles using a climatic chamber (model DM340C by Angelantoni Industrie Srl, Perugia, Italia), in a temperature interval from 16 to 31 °C, according to the scheme reported in Fig. 3. The testing temperatures were chosen according to the climatic data of Meteotrentino (https://www.meteotrentino.it) measured in Trento (Italy) during the summer seasons of the years 2019, 2020 and 2021: the minimum temperatures during this period were 17.2 ± 3.0 °C, 16.9 ± 2.0 °C and 16.3 ± 2.2 °C, respectively; the maximum temperatures were 29.4 ± 4.0 °C and 29.0 ± 3.2 °C and 28.4 ± 3.3 °C, respectively. The temperature values as function of time were recorded using an RS Pro Temperature Datalogger equipped with type-K thermocouples: three thermocouples were located inside the box and one outside in order to record the temperature profile of the climatic chamber. During the test the boxes were placed on an expanding polystyrene (EPS) basement, 10 cm thick, in order to avoid any heat transfer to/from the testing boxes. For each box three heating/cooling sequences were performed, with a total testing time of around 75 h. The boxes used for the test are shown in Fig. 2.

The maximum (T_{max}) and the minimum temperature (T_{min}) reached within each box and from the chamber were determined, as well as the time required to reach a temperature of 26 °C (t_{26}) and a temperature of 18 °C (t_{18}) starting from the lowest temperature (T_{min}).

The distribution of paraffin within the elastomeric matrix was verified by monitoring the surface temperature of the EPDM + RT28 + ENV and EPDM panels through an IR thermal camera FLIR E60 (emissivity = 0.95). The specimens were preconditioned in an oven at 35 °C overnight and then inserted in the climatic chamber at a temperature of 22 °C. Thermograms of the sample's surfaces were acquired after 30 and 60 min from the beginning of the test. In the same way, the specimens were cooled at 22 °C overnight and then inserted in an oven at a temperature of 35 °C. IR images of the sample's surfaces were acquired after 30 and 60 min from the beginning of the test.

3. Results and discussion

In Fig. 4 (a-c) the results of the rheometric measurements, viscometric measurements for the determination of Mooney viscosity and of Mooney scorch time are reported, respectively. The results are summarized in Tables 3-5.

Observing the viscosity curves (Fig. 4a) and their results (Table 3), it is possible to notice that the two materials are characterized by similar values of torque peak, that in the case of EPDM + PCM decreases once paraffin starts melting, reaching a plateau that is maintained for the whole duration of the test. The resulting ML (1 + 4) viscosity highlights the influence of paraffin with a value of 50.4 MU in the case of EPDM and 11.4 MU in the case of EPDM + PCM.

From the viscosity curves generated to obtain the scorch time (Fig. 4b) and their results (Table 4), it is possible to observe that, after the torque peak, the sample EPDM + PCM is characterized by an extended plateau at low torque values (2 MU) and it is unable to reach higher values. This behaviour is probably caused by the melting of paraffin (occurring in correspondence of the torque' drop) that acts as lubricating agent. On the contrary, the EPDM sample is characterized by a torque minimum of 18 MU, by a t_5 of 12.1 min and t_{35} of 22.5 min. These tests confirms that the working conditions during the production process of the material are safe, since at least 12.1 min are required at a temperature of 130 °C in order to start the vulcanization process of the compound.

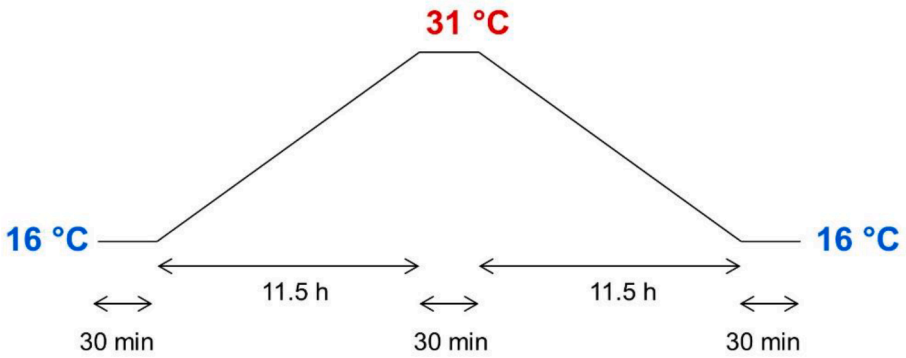

Fig. 3. Temperature profile applied in the climatic chamber.

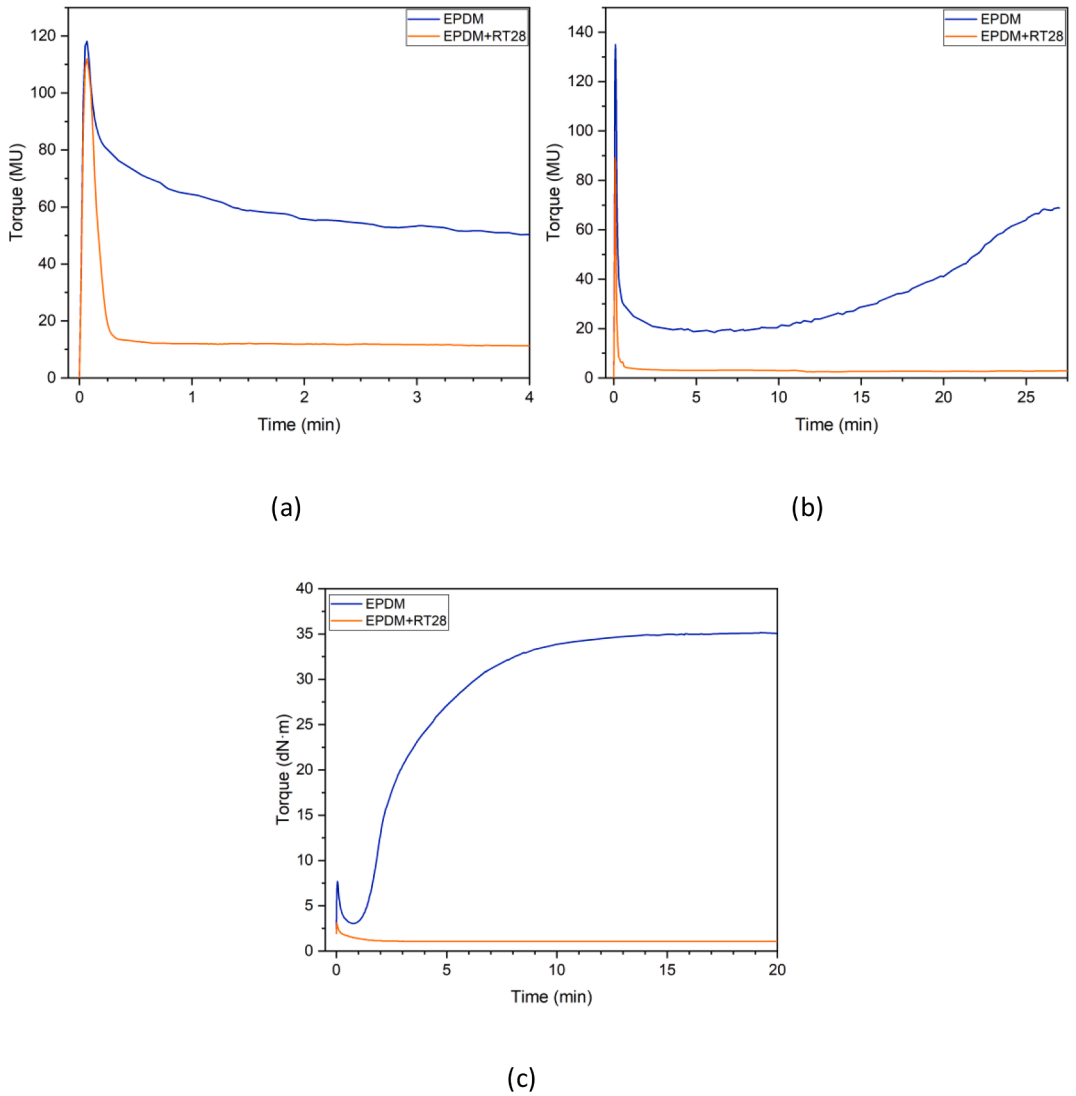

Fig. 4. Viscometric curves at 100 °C for the determination of Mooney viscosity (a), viscometric curves at 130 °C for the determination of Mooney scorch time (b) and rheometric curves at 184 °C for EPDM and EPDM + RT28 samples (c).

Table 3
Results of viscosity measurements at 100 °C.

Sample	ML (1 + 4) [MU]
EPDM	50.4
EPDM + RT28	11.4

Table 4
Results of Scorch time measurements at 130 °C.

Sample	ML [MU]	t_5 [min]	t_{35} [min]
EPDM	18	12.1	22.5
EPDM + RT28	2	–	–

Observing the rheometric curves (Fig. 4c) and their parameters (Table 5), the difference between the two samples is clear. The EPDM sample shows the typical behaviour of elastomers during the vulcanization with a considerable difference between the ML and MH values due to the formation of sulphur bonds. On the other hand, the EPDM + PCM show very low torque values, without any increase: this behaviour

Table 5
Results of rheometry measurements at 184 °C.

Sample	ML [dN·m]	MH [dN·m]	t_{s2} [min]	t_{90} [min]
EPDM	3.07	34.15	1.2	7.4
EPDM + RT28	1.06	–	–	–

is due to the plasticizing effect of paraffin that, diluting the elastomer, hinders the vulcanization process due to the excessive distance between the polymer chains of the elastomer. The EPDM sample is characterized by a t_{s2} value of 1.2 min, by a t_{90} of 7.4 min and by a maximum torque of around 34 dN·m.

Vulcanized samples have been then characterized according to different techniques in order to investigate the ability to retain paraffin, the microstructure of the samples, the thermal and mechanical properties and the TES efficiency. In order to evaluate the ability of the NBR envelope to avoid paraffin leakage, a double cycling test was performed. From the results reported in Table 6, it is possible to observe that in the first sequence no paraffin loss occurred, as the residual PCM content is equal to the initial one (i.e., 56.8 wt%), while in the second one the PCM loss was very limited (around 1.3 %), with a final PCM content of around

Table 6
Results of leakage test.

Sample	Initial PCM content [wt%]	Paraffin loss 1 [wt%]	Residual PCM content 1 [wt%]	Paraffin loss 2 [wt%]	Residual PCM content 2 [wt%]
		sequence 1		sequence 2	
EPDM + RT28 + ENV	56.8	0	56.8 ± 0.0	1.3	55.5 ± 0.2

55 wt%. It can be therefore concluded that the insertion of a NBR envelope represents a valuable technique to prevent PCM leakage at the molten state.

From the SEM pictures of EPDM sample, presented in Fig. 5 (a,b), it is possible to observe that the material is compact and the morphology uniform. EPDM + PCM sample (Fig. 5 (c,d)) is characterized by the absence of voids or porosity with the paraffin that is homogeneously distributed on the sample surface forming a white layer on the sample surface. Comparing the SEM micrographs of EPDM and EPDM + PCM samples, it is possible to observe that the addition of paraffin slightly modifies the morphology of the EPDM rubber, with the fracture surfaces that show the plasticizing effect of the PCM.

From the results of density measurements, reported in Table 7, it is possible to observe that the addition of paraffin leads to a decrease of the density from 1.01 g/cm^3 (EPDM) to 0.94 g/cm^3 (EPDM + RT28), partially compensated by the presence of clay in the compound. In the

Table 7
Results of density measurements.

Sample	ρ_{geom} [g/cm^3]
EPDM	1.01 ± 0.03
EPDM + RT28	0.94 ± 0.01
EPDM + RT28 + ENV	1.02 ± 0.04

EPDM + RT28 + ENV, the presence of the NBR envelope, leads to an increase of the density that reaches values of around 1.02 g/cm^3. However, taking into account the standard deviation values associated with the measurements, it is possible to conclude that the density of the three samples is quite similar.

Thermogravimetric analysis of EPDM, RT28 and ENV samples were performed in order to understand the influence of each component on the degradation of EPDM + RT28 and EPDM + RT28 + ENV. Thermogravimetric curves, along with the corresponding derivative curves are presented in Fig. 6 (a, b), while the most interesting results are reported in Table 8.

From the thermogram of neat paraffin it is evident that the degradation takes place in a single step at about 213 °C (corresponding to T_{peak1}), starting at around 150 °C ($T_{5\%}$). EPDM shows three main degradation steps, related to the degradation of the polymeric matrix at about 450 °C (T_{peak2}) and to the decomposition of the carbonaceous fillers at 630 °C (T_{peak3}). A minor degradation step caused by oils and low molecular weight plasticizer can be identified at around 200 °C. A similar behaviour can be observed in the case of the NBR sample (ENV),

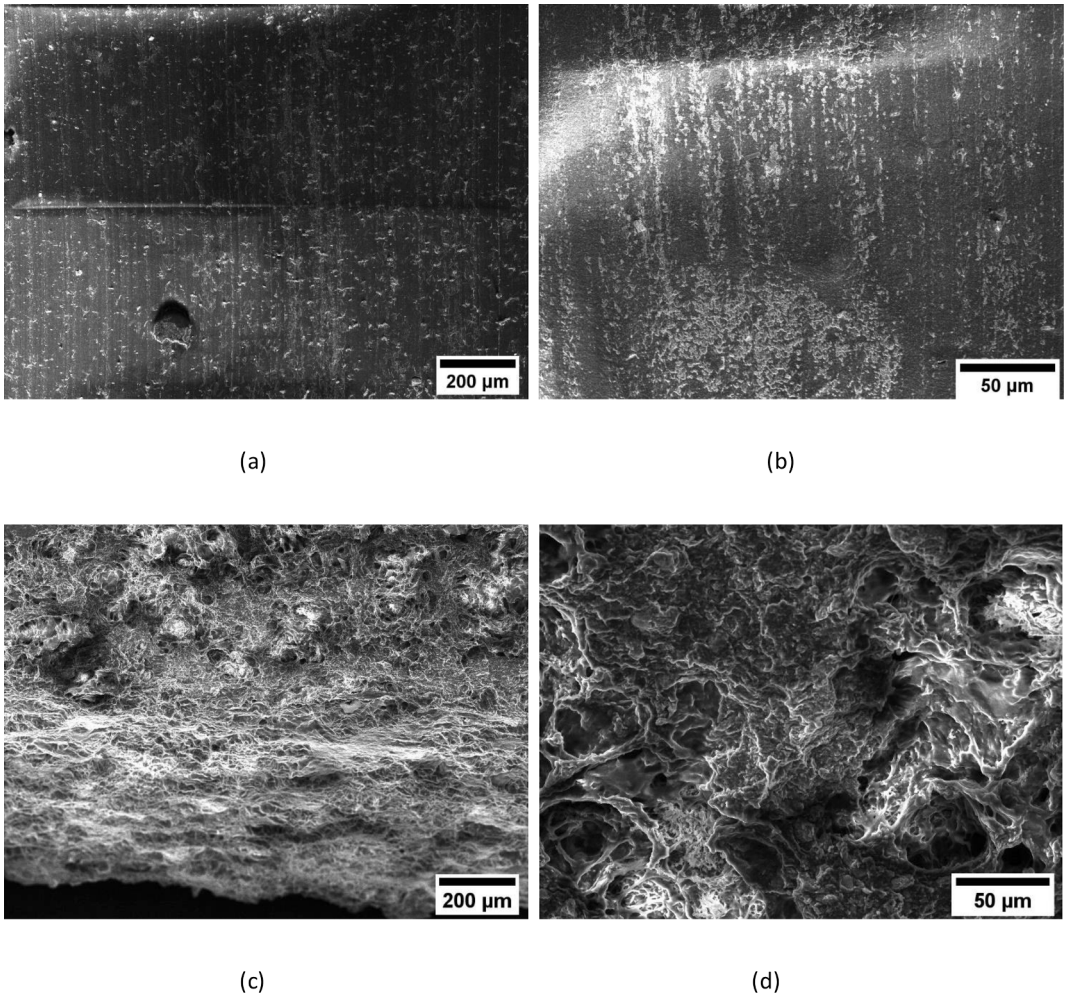

Fig. 5. SE-SEM micrographs on the EPDM (a,b) and EPDM + RT28 (c,d) samples at different magnifications: 200x (a,c) and 1000x (b,d).

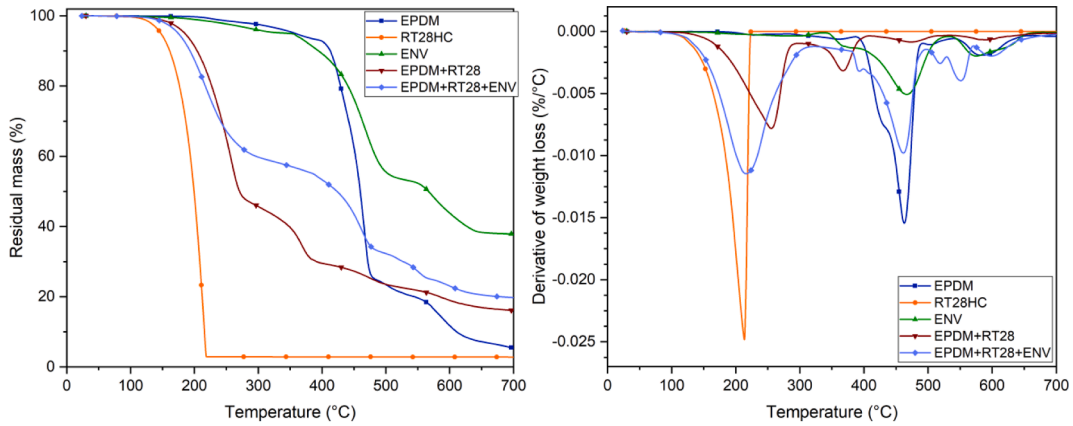

Fig. 6. Thermogravimetric analysis curves: residual mass (a) and derivative of weight loss (b).

Table 8
Results of TGA tests on the single constituents, on EPDM + RT28 and EPDM + RT28 + ENV samples.

Sample	$T_{5\%}$ [°C]	T_{peak1} [°C]	T_{peak2} [°C]	T_{peak3} [°C]	m_{700} [%]
EPDM	358.0	–	463.0	581.8	5.4
RT28HC	147.5	213.4	–	–	2.8
ENV	348.7	–	467.2	575.2	37.8
EPDM + RT28	185.2	255.5	367.3/ 471.7	590.3	16.2
EPDM + RT28 + ENV	174.8	216.1	461.4	551.1/ 598.4	19.8

which is characterized by a $T_{5\%}$ of around 348 °C, by a T_{peak2} of 467 °C and by a T_{peak3} of 575 °C. The main difference between the two elastomers is that a higher residual mass content was detected in the case of ENV (37.8 %) due to the presence of around 33 wt% of inorganic fillers in its composition (talc, kaolin and silica). Observing the curve of EPDM + RT28, it is evident that the addition of paraffin leads to a decrease of the thermal stability of the material. In particular, the $T_{5\%}$ decreases from 358 °C of EPDM to 185 °C; the curve then follows a slightly different behaviour with respect to that observed for neat EPDM, with the elastomeric matrix reaching the maximum degradation speed at two different temperatures (367 and 472 °C). The T_{peak3} occurs at around 590 °C, similarly to the EPDM sample. The EPDM + RT28 + ENV sample is characterized by a lower thermal stability with respect to the EPDM + RT28: the $T_{5\%}$ occurs at around 175 °C and the T_{peak1} at around 216 °C. Its thermal degradation is thus influenced by both EPDM and NBR rubber: T_{peak2} occurs at around 460 °C (but a small peak can be detected at about 380 °C) and T_{peak3} can be identified at 551 °C (with a small peak at around 600 °C). The m_{700} value of EPDM + RT28 (16.2%) is rather high, if compared with that of EPDM and RT28HC, due to the presence of Cloisite20 that was added as shape-stabilizer. As reported in Table 2, its amount is around 15 wt%: considering a residual mass of 5.4 wt% for EPDM and of 2.8 wt% for paraffin, it can be evaluated that the residual mass of EPDM + RT28 should be around 9.3 g, that compared to the initial mass (51 g, see Table 2), is equal to 18 wt%, very similar to the 16.2 wt% reported in Table 8. The m_{700} value of EPDM + RT28 + ENV (19.8 wt%) is coherent if compared with that of ENV and EPDM + RT28 samples: considering, according to Table 2, an EPDM + RT28 mass of 47 g and an ENV mass of 18 g and a residual mass of 16.2 wt% and 37.8 wt %, respectively (according to Table 8), it results that the residual mass of EPDM + RT28 + ENV should be of around 14.2 g, corresponding to 21 wt%, very similar to the 19.8 wt% reported in Table 8.

Considering the mass loss between 150 and 250 °C, it is possible to evaluate the paraffin content of the samples EPDM + RT28 and EPDM + RT28 + ENV: it results that the paraffin amount should be around 50 wt % in the first case and around 40 % in the second one. In the case of EPDM + RT28 + ENV, the value is coherent with the one that can be calculated using the data reported in Table 2 (around 41 wt% of paraffin with respect to the total sample mass, considering the envelope). In the case of EPDM + RT28, the value is lower with respect to the theoretical one (around 57 wt%): the reason for this lower paraffin amount could be related to a certain paraffin degradation during the vulcanization process, more pronounced in the case of EPDM + RT28 sample due to the absence of the protective NBR envelope.

In order to evaluate the role of paraffin on the thermal properties of the samples, DSC tests were performed. The DSC thermograms are presented in Fig. 7 (a-c), while the most important results are listed in Table 9.

From the thermograms it is evident the melting peak of paraffin at around 25 °C, whose intensity is proportional to the paraffin content. It is possible to observe that the main melting peak of paraffin is narrower and sharper in comparison to those present in EPDM + RT28 and EPDM + RT28 + ENV samples. The same behaviour can be observed in the cooling scan, where the elastomeric samples present a slight shift of the crystallization temperature (T_c), which is about 4–5 °C lower with respect to that of neat paraffin. In the second heating scan, the melting temperature (T_{m2}) is the same for all the samples, probably thanks to the cooling scan carried out at a low speed. The enthalpy of transition was found constant during the thermal cycle of heating–cooling-heating, i.e. about 126 J/g for EPDM + RT28, and 97 J/g for EPDM + RT28 + ENV, proportionally lower than 263 J/g of single paraffin.

Considering the effective PCM content, it is possible to observe that no differences can be observed between the first and the second heating scan, meaning that the PCM is stable within the elastomeric matrix and free of melting and crystallizing. The values of PCM_{m2}^{eff} are around 48 wt % for EPDM + RT28, and 37 % for EPDM + RT28 + ENV. It is possible to compare these values with the estimated paraffin content evaluated from the results of TGA analysis: a PCM_{m2}^{eff} content of 50 wt% and 40 wt% can be respectively detected for EPDM + RT28 and EPDM + RT28 + ENV samples, very similar to those obtained in DSC tests. As already observed for TGA, these values can be compared to the theoretical ones reported in Table 2 (57 wt% and 41 wt%, respectively): they are lower in the case of EPDM + RT28 probably due to paraffin degradation during the vulcanization process, but almost equal in the case of EPDM + RT28 + ENV thanks to the presence of the envelope that hinders paraffin degradation during the vulcanization process.

From the results of the Shore A hardness test reported in Table 10, it

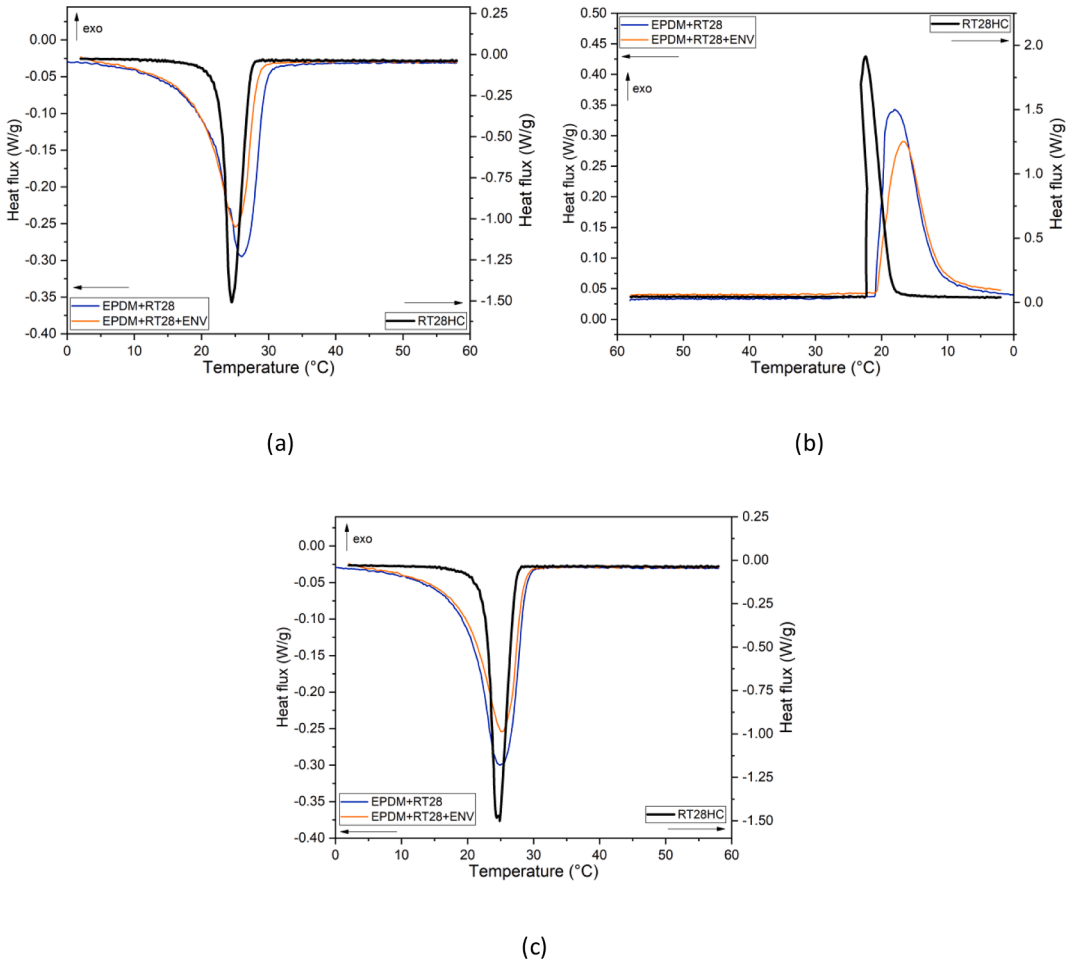

Fig. 7. DSC curves at 1 °C/min: first heating scan (a), cooling scan (b) and second heating scan (c).

Table 9
Selected results of DSC at 1 °C/min.

Sample	T_{m1} [°C]	ΔH_{m1} [J/g]	P_{heat} [J/cm^3]	PCM_{m1}^{eff} [%]	T_c [°C]	ΔH_c [J/g]	P_{cool} [J/cm^3]	PCM_c^{eff} [%]	T_{m2} [°C]	ΔH_{m2} [J/g]	PCM_{m2}^{eff} [%]
RT28HC	24.4	263.2	202.7	100	22.4	262.3	230.8	100	24.5	262.9	100
EPDM + RT28	26.0	125.6	118.1	47.7	18.0	125.7	118.2	47.9	24.9	125.8	47.8
EPDM + RT28 + ENV	25.0	96.7	98.7	36.7	16.7	96.8	98.7	36.9	25.1	96.9	36.9

can be observed a strong dependency from the testing temperature in the case of the EPDM + RT28 + ENV panel. In particular, Shore A value below the T_m is around 83, with paraffin acting as hardener, while above the T_m there is a drop until a value around 23 due to the softening effect of melted paraffin. This behaviour, already observed in the case of EPDM foams containing paraffin, should be taken into account in order to select this material on the basis of the mechanical performance required for a certain application, in order to avoid softening problems above the T_m of paraffin [37]. On the other hand, the surface hardness of the EPDM panel (Shore A around 58) is not influenced by the testing temperature.

Compressive curves of EPDM and EPDM + RT28 + ENV panels below and above the melting point of paraffin are shown in Fig. 8 (a-b), while the most important results are listed in Table 11. The compressive properties of the EPDM panel do not seem to be influenced by the temperature: the shape of the two curves is the same and the values of elastic modulus, $\sigma_{0.1}$ and $\varepsilon_{0.1}$, considering the standard deviation values, are practically identical. Interestingly, the compressive behaviour of the EPDM + RT28 + ENV panel is considerably influenced by the testing temperature due to the presence of paraffin: in particular, the elastic modulus decreases from 2.7 MPa (at 10 °C) to 2.1 MPa (at 40 °C). At 40 °C the material is very soft and, as shown in Fig. 8b, is unable to sustain high load values, reaching a max compressive stress of about 0.25 MPa: this behaviour is due to the rupture of the external envelope and the consequent flow-out of the internal EPDM + RT28 compound. Considering a possible application on the floor, it can be estimated a walking pressure of around 0.08 MPa (foot surface area ~ 98 cm^2, weight 80 kg = 784 N), well below the maximum compressive stress sustained from the panel.

On the contrary, at 10 °C, the material is harder and able to sustain load without any damage to the external envelope. Looking at the $\sigma_{0.1}$ and $\varepsilon_{0.1}$ values, it is possible to observe that only very small differences

Table 10
Results of shore A hardness test.

Sample	Shore A T = 0 °C	Shore A T = 40 °C
EPDM	57.5 ± 1.2	58.3 ± 1.4
EPDM + RT28 + ENV	82.7 ± 5.0	22.8 ± 1.6

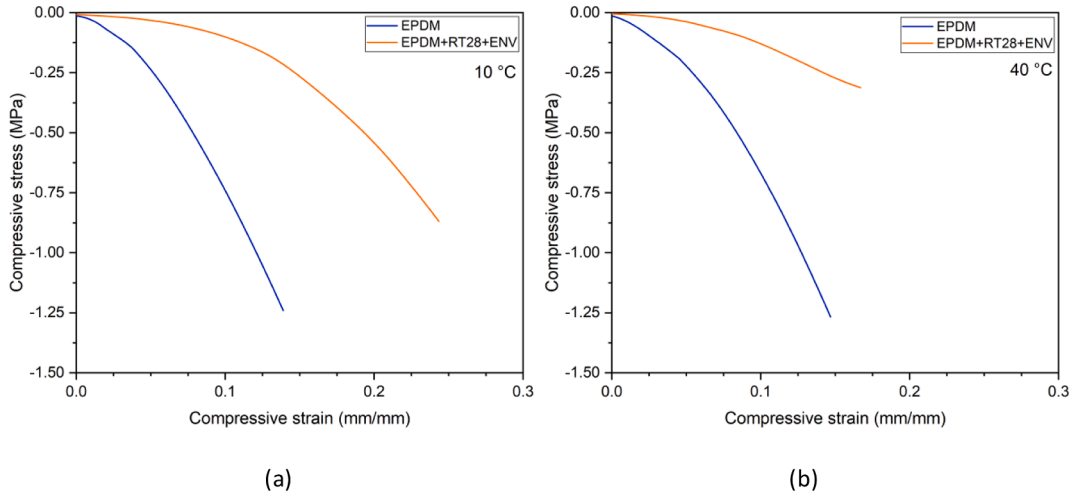

Fig. 8. Representative stress–strain curves, at 10 °C (a) and at 40 °C (b) from quasi-static compression tests.

Table 11
Results of quasi-static compression tests.

Sample	E at 10 °C/at 40 °C [MPa]	$\sigma_{0.1}$ at 10 °C/at 40 °C [MPa]	$\varepsilon_{0.1}$ at 10 °C/at 40 °C [mm/mm]
EPDM	8.31 ± 1.78 / 7.07 ± 1.62	0.61 ± 0.14 / 0.52 ± 0.13	0.03 ± 0.01 / 0.04 ± 0.01
EPDM + RT28 + ENV	2.68 ± 0.91 / 2.10 ± 0.87	0.09 ± 0.03 / 0.20 ± 0.05	0.11 ± 0.02 / 0.06 ± 0.02

occur below and above the melting point of paraffin: at 40 °C slightly higher values of $\sigma_{0.1}$ and lower values of $\varepsilon_{0.1}$ are measured, meaning that in the first part of the curve the higher temperature seems to decrease the length of the plateau with a more rapid stress increase that then is limited at lower values with respect to the curves obtained at 10 °C.

From the results of the thermal conductivity test reported in Table 12, it is possible to observe that the EPDM panel is characterized by slightly lower thermal conductivity (around 0.11 W/m·K) with respect to the EPDM + RT28 + ENV panel (around 0.15 W/m·K): the presence of paraffin, whose declared thermal conductivity is around 0.20 W/m·K, results in a higher thermal conductivity for this panel [55]. Comparing the values obtained through heat flux meter at different temperatures, it is possible to identify only a small decrease of the thermal conductivity that is around 0.17 W/m·K at 10 °C, and around 0.15 W/m·K at higher temperatures: the presence of solid or liquid paraffin within the EPDM + RT28 + ENV panel seems, thus, to not influence the global behaviour of the material in terms of thermal conductivity.

Looking at the thermal conductivity values obtained using the hot-disk technique, it is possible to observe that higher values were measured: in particular, the thermal conductivity of EPDM is around 0.28 W/m·K, while the one of EPDM + RT28 + ENV reaches values of around 0.66 W/m·K. This difference can be due to the different working principles of the two techniques (the HFM is a steady-state technique, while the hot disk is a method based on the temperature transient), as observed in other works [56,57]. In particular, Weingrill et al. observed that the thermal conductivity of polyethylene samples measured using the hot disk technique, was systematically higher with respect to the thermal conductivity measured with a guarded heat flow meter test method [56].

Table 12
Results of thermal conductivity test.

Sample	HFM-10 °C [W/m·K]	HFM-30 °C [W/m·K]	HFM-40 °C [W/m·K]	Hot-disk [W/m·K]
EPDM	0.110 ± 0.023	0.113 ± 0.023	0.115 ± 0.023	0.278 ± 0.004
EPDM + RT28 + ENV	0.175 ± 0.053	0.152 ± 0.026	0.150 ± 0.021	0.657 ± 0.054

Fig. 9 reports the result of the thermal cycling test on wood boxed insulated with panels of EPDM and EPDM + RT28 + ENV. In the heating stage, the temperature of the box insulated with EPDM increases with the same trend of the climatic chamber; on the other hand, the temperature increase of the box insulated with EPDM + RT28 + ENV slows down starting from 24 °C, reaching a plateau at around 27 °C until the temperature of the chamber starts to decrease. The temperature plateau corresponds to the nominal melting point of this paraffin (around 28 °C, according to the technical data sheet), and is slightly higher with respect to that evaluated from DSC analysis (about 25 °C). The reason for this slight discrepancy is probably the very low testing speed selected for this test. It was already observed, in DSC tests, that the reduction of the testing speed causes the shift of the melting peaks through the theoretical value (28 °C in this case) [37].

In the cooling stage the two boxes have the same behaviour, with the one containing paraffin that has a small delay due to the temperature plateau reached during the heating. The same behaviour was observed

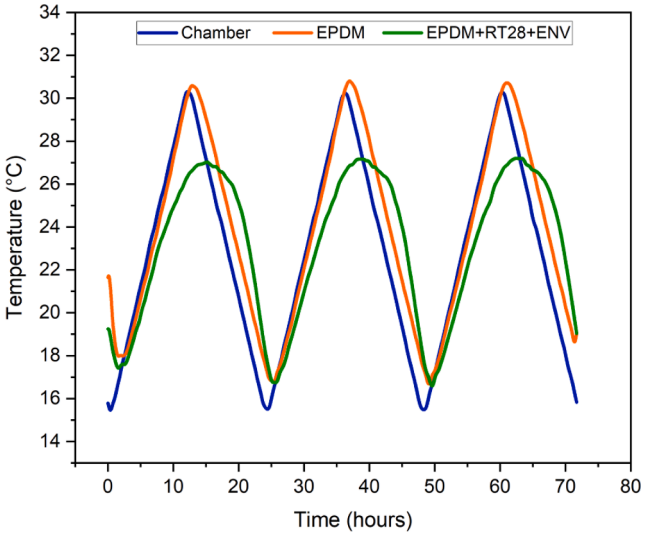

Fig. 9. Evaluation of the thermal energy storage capability of the wood boxes: trend of the internal box temperature in cycle test within three days.

also in the second and third heating cycles, confirming the repeatability of these tests.

From the results summarized in Table 13, it is possible to observe that the box insulated with EPDM reaches a maximum temperature of 30.4 °C while the box insulated with EPDM + RT28 + ENV reaches a maximum temperature of 27 °C, with a time delay of more than 1 h required to reach the temperature of 26 °C (t_{26}), slightly lower in cooling (t_{18}). This behaviour is very interesting in the case of building applications: the usage of such insulating panels in certain climatic regions (like Trento, Italy) may allow the reduction of the maximum temperature reached by the building's envelope in the summer period. The proper selection of the melting temperature of the PCM could thus lead to a consistent reduction of the energy consumption for air conditioning in the summer period. In order to evaluate the long-term performances of the insulating box, a similar lab scale test repeated after 15 months confirmed the thermal energy storage ability, and the durability of the EPDM + RT28 + ENV sample: the T_{max} was decreased of 4.0 °C with respect to the peak temperature of the chamber, and a similar delay either in heating or in cooling was observed.

From the pictures obtained with the IR camera, reported in Fig. 10 (a-d), it is possible to observe the temperature uniformity on the surface of EPDM + RT28 + ENV panel that confirms the good distribution of paraffin obtained in the production process. The pictures, acquired both during heating and cooling after 30 and 60 min, highlight the temperature difference between the EPDM and the EPDM + RT28 + ENV panels, with the second one that shows lower (or higher) temperatures even after a test duration of 1 h.

4. Heating and cooling applications of PCMs in the medium–low temperature range and future perspectives

In medium–low temperature ranges, applications involving PCMs are widely documented in scientific literature. In the last years, relatively low temperature ranging from about 10 °C to 40 °C, have received an increasing attention as potential solution in energy buildings technologies specifically to fill the energy gap between supply and demand load in Heating, Ventilation and Air Conditioning (HVAC). Table 14 summarizes suitable cases selected in literature to be compared with the results of the present study. They are referred to different materials suitable for specific building applications and are furthermore detailed for testing methodology (typically heating and cooling) and temperature range.

Reference is made to the work of Kasaeian et al. [58] for a review of the applications pertaining the HVAC sector. In the first part of this paragraph, a selection of significant cases investigating the impact of PCMs in energy buildings performances is proposed. Reference is made to the corresponding bibliography for a detailed analysis. For clearness, the study cases selected for comparison include investigations referred both experimental and modelling point of view. It is important to underline that providing the design guidelines in terms of mathematical modelling and simulation techniques represents an expected need to turn the fundamental experimental PCMs research, as that provided in this work, towards deep engineering applications. Looking at the actual energy buildings perspectives, PCMs placed inside the structure and/or the envelope of the buildings structure constitute, actually, one of the most extended application to enhance both the energy performances and the thermal comfort of buildings.

For passive cooling in buildings, the study of Kong et al. [59] demonstrates that the use of expanded perlite based PCM wallboards reduces the peak temperature of the inside wall surface by 7.0 °C and the average air temperature of the monitored rooms of 2.4 °C. Yao et al. carried out a similar investigation by analysing an office building presenting an area of 4000 m^2. In this application, a PCM wallboard made of a mixture of expanded perlite and paraffin with a melting point within 25–29 °C, has allowed to achieve a reduction of 9.2 °C of the average temperature of the office during the working time from 7:00 a.m. to 6:00 p.m. Thermal impacts of PCMs have been investigated by Lee et al. [61] by carrying out tests on a wall construction including a PCM wallboard presenting a typical residential geometry. The selected paraffin-based PCM, presenting a melting temperature of 28 °C and TES of 69 kJ/kg, allows to achieve an average delayed time of 1.5 h of the peak heat flux and, correspondently, a 25.4 % average reduction of the daily heat flux. Furthermore, PCMs wallboards can represent a promising solution for room thermal energy storage (TES) when incorporated into floors and roofs. The benefit consists in increasing the heat storage capacity to reduce the indoor temperature in particular in warm climates. The experimental study of Entrop et al. [62] demonstrated that, after incorporating a PCM wallboard having a melting point of 23 °C into the concrete floor, the temperature difference reduces from 2.8 to 4.2 °C without PCM and from 0.1 to 1.5 °C with PCM using light or heavy insulation respectively.

Similar results have been obtained by Cabeza et al. [63] and Barzin et al. [64] evaluating the global energy saving performances of an innovative concrete incorporating PCMs with a melting point of 26 °C. The work of Barzin et al. is specifically referred to an experimental investigation combining wallboards in floor heating by making use of paraffin based PCMs with a melting point of 28 °C. This study includes, as final results, the impact of the adopted solution on the total energy and electricity costs saving which amounts, for the analysed periods, to 18.8 % and 28.7 % respectively.

The second part of this paragraph includes a synthetic presentation of advanced applications of PCMs concerning, in particular, their integration into TES technologies. Due to the increase of heating and cooling loads in buildings, this research subject is nowadays receiving particular attention as proved by the relevant number of emerging studies as emerges from the work of Raza et al. [65] to which reference is made for a broad overview.

One of the most investigated topics pertains the use of PCMs as based storage systems integrated with solar thermal plants. Daghigh and Shafieian [66] evaluate the energy and exergy efficiency of evacuated solar tube collectors utilized for space heating. These solar devices have been integrated with PCM to accumulate extra energy amounts that could also find different uses. In particular, the Authors had laid significant stress on the economic impact of the proposed solution. A similar study, specifically dealing with the use of PCMs as TES to cover residential heating demand, has been investigated by Ling et al. [67].

Zhang et al. [68] have carried out an experimental investigation covering the years 2011–2014 in view of evaluating the radiant plants performances when connected to solar systems including PCMs. The proposed solution has allowed to maintain the temperature of the rooms 5–7 °C higher. In particular, compared to conventional solar plants, the integration with PCMs (based of paraffin and HDPE with TES = 144 kJ/kg) has enhanced the performances of the global plant up to 30%. Advanced solutions involve the direct integration of PCMs into solar collector devices as those proposed by Koca et al. [69]. In this case the solar unit comprises the collectors integrated with a storage working with Mobil term 605 as thermal carrier to transfer heat from the solar collectors to the utilized PCM (CaCl2·6H2O). Based on the monitored experimental campaign performed in October, the proposed solution allowed to increase the global efficiency of the plant up to 45 %. Similar purposes have been pursued by Arkar et al. [70] by investigating an innovative design of an evacuated tube solar collector (ETSC) including

Table 13
Results of the test for the evaluation of the thermal energy storage ability.

Sample	T_{max} [°C]	T_{min} [°C]	t_{26} [hours]	t_{18} [hours]
Chamber*	30.7 ± 0.1	15.5 ± 0.1	11.9 ± 0.1	22.0 ± 0.1
EPDM	30.4 ± 0.1	15.4 ± 0.5	12.0 ± 0.2	23.7 ± 0.1
EPDM + RT28 + ENV	27.1 ± 0.1	16.8 ± 0.2	13.2 ± 0.3	24.2 ± 0.1

*Chamber = temperature of the climatic chamber.

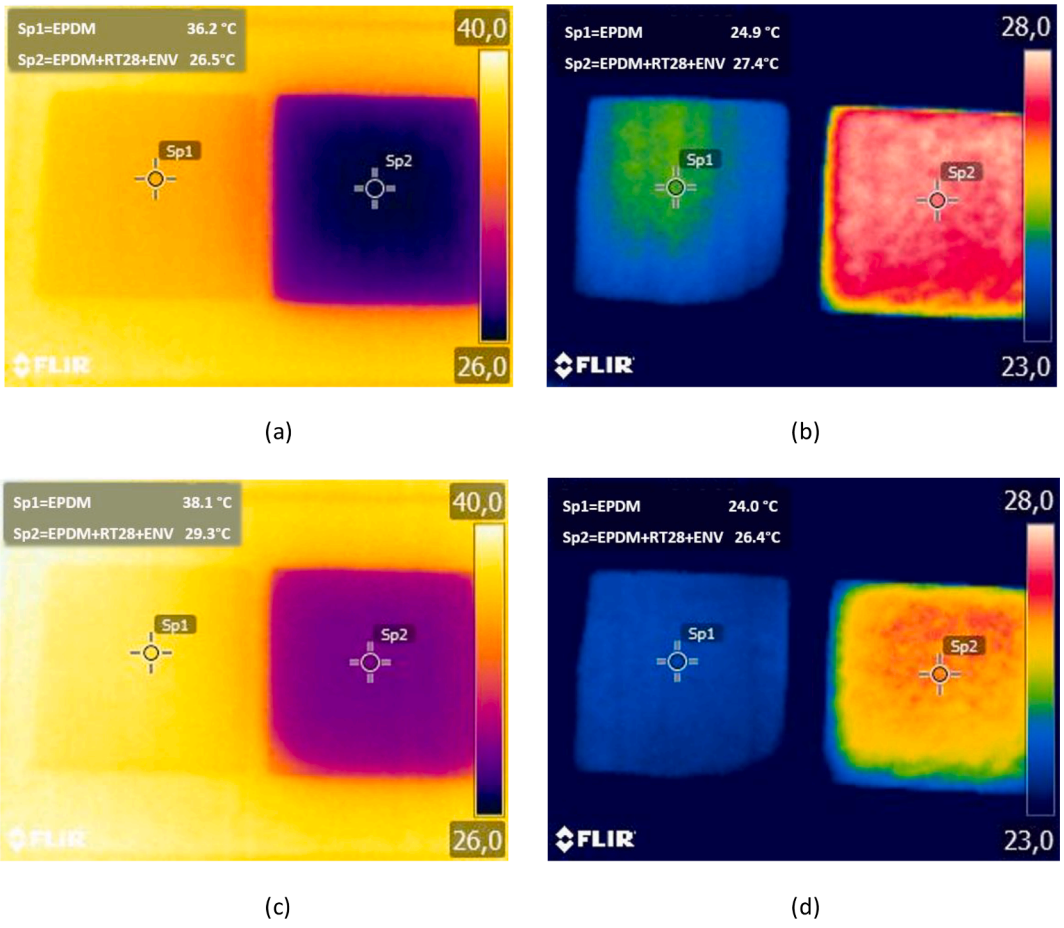

Fig. 10. Thermograms obtained through IR camera during heating (a,c) and cooling (b,d), after 30 min (a, b) and 60 min (c, d).

Table 14
Comparative evaluation of TES systems for building applications.

Type of test*	Temperature interval	$TES_{W/S}$ **	Material	Application	System	Latitude (country)	Notes	Ref.
H, C	20–40 °C	86 kJ/kg	paraffin in expanded perlite	wallboard, roof	multilayer	China	real conditions on small houses	Kong et al. (2017) [59]
–	25–29 °C	65–69 kJ/kg	paraffin in expanded perlite - graphite	wallboard	single layer	China	application to office building	Yao et al. (2018) [60]
H, C	25–65 °C	69 kJ/kg	paraffin in cellulose	wallboard	blowing in cavities	US (DOE region 4)	real conditions on small houses	Lee et al. (2018) [61]
H, C	20–30 °C	5.4 kJ/kg	paraffin in aluminium case	wallboard (Energain)	multilayer	Twente (The Netherlands)	real conditions on small houses	Entrop et al. (2011) [62]
H, C	15–35 °C	5.5 kJ/kg	PCM in concrete	wall-roof-floor	massive	Lleida, Spain	real conditions on small houses	Cabeza et al. (2007) [63]
H, C	30–50 °C	70 kJ/kg	Paraffin panel coupled with gypsum board	PCM wall board (Energain) and floor	multilayer	Auckland, New Zealand	Dedicated experimental huts	Barzin et al. (2015) [64]
H, C	5–40 °C	97 kJ/kg, 504 kJ/m^2	paraffin in rubber	wall	multilayer	Trento, Italy	delay in H/C rate	This paper (2021)
H, C	10–50 °C	144 kJ/kg	PCM (paraffin -graphite-HDPE) in storage tank	PCM accumulation + solar panels	Vertical storage (tank)	China	integration to floor heating system	Zhang et al. (2016) [68]
H, C	–	187 kJ/kg	$CaCl_2$ $6H_2O$ in a storage tank	PCM accumulation + solar panels	tank	Turkey	energy/exergy study	Koca et al. (2008) [69]
H, C	15–40 °C	86 kJ/kg	microencapsulated PCM within 2 concentric Al tubes	PCM accumulation + solar panels	storage (tank)	Ljubljana, Slovenia	air vacuum tube solar collector and a concentric-tube	Arkar et al. (2016) [70]
H, C	35–55 °C	300 kJ/kg	KNO_3 + 0.46 $NaNO_3$	floor heating and solar panel	tank	Melbourne, Australia	accumulation tank connected to solar panel	Zhao et al. (2017) [71]

*H: heating / C: cooling; ** $TES_{W/S}$ thermal energy storage by weight or by surface.

a latent heat thermal energy storage system (LHTES). Making reference to the case of buildings presenting a heating load of 34 kWh/m^2, the proposed LHTES system allows to capture about the 63 % of the solar incident fraction.

Modelling studies can be found in this issue as the parabolic trough collector model developed by Zhao et al. [71] where Nitrate Salt (0.54 KNO_3 + 0.46 $NaNO_3$) is used as PCM for the proposed simulation applied to floor radiant heating systems. The model, tested on winter and summer conditions yearly basis, demonstrated that the proposed PCM solution satisfies the required energy load even during off sunshine hours (7p.m.-5 a.m.) by releasing the thermal energy stored during daytime.

In recent years, particular attention has been dedicated to innovative TES solutions by integrating Photo Voltaic-Thermal (PV-T) solar collectors with PCMs. Considering that the latent heat of fusion is greater with respect to the specific heat, this option provides an increase of electrical and thermal gain. As investigated by Hasan et al. [72], the adopted technology allows the power production to increase by 5.5 % as average value due to the reduced working temperature of the PV collectors that entails an increase of the open-circuit voltage. The integration of PCMs looks particularly attractive to achieve this goal as confirmed by recent research works [73,74,75] that demonstrate that this solution enhances both thermal and electrical performances. From the proposed examples, although providing a limited review of the cases till now studied, the utilization of PCMs emerges as a strategic solution to drive the energy saving strategies of buildings technologies [76,77]. The use of PCMs seems also very promising for the thermal management of refrigerated vehicles: their use in the walls of trucks has been demonstrated to be a successful strategy to reduce both peak and heat transfer [78]. Some research gaps highlight the lack of consolidated procedures to evaluate important parameters for energy building performances (wall thickness, location of building, geometry of building, selection of PCM etc.) and constitute an interesting challenge for future investigations.

It is clearly evident that these PCM rubber panels investigated in this work represent a unique case of study in scientific literature of application dedicated to thermal energy storage. This preliminary analysis could represent a significant novelty not only in building applications but also in other fields where specific elastomeric properties are required in the temperature range 0–40 °C. It should be properly considered the maximum allowable compressive stress of 0.25 Mpa at 40 °C, due to the undesired leakage of paraffin.

5. Conclusions

In this work, the preparation and characterization of EPDM/NBR panels containing paraffin for thermal energy storage applications has been reported for the first time. The prepared panels present a thickness of 5 mm, a density of 1.02 g/cm^3 and a grammage of 5200 g/m^2. Viscosity curves performed on EPDM and EPDM + RT28 highlighted the influence of paraffin on the behaviour of the elastomeric compound that was characterized by very low values of torque after melting of paraffin. In the same way, the rheometric curves evidenced the influence of paraffin that seemed to hinder the vulcanization of the compound. Leaking tests on the prepared panels revealed the optimal barrier properties of the external NBR envelope: a paraffin loss of only 1 % after two test sequences lasted around 3 months was detected. SEM observations highlighted the homogeneous distribution of paraffin within the elastomeric matrix, that was also confirmed by pictures taken with an IR camera during heating/cooling cycles. The effective PCM content evaluated through DSC analysis performed at ± 1 °C/min was around 37 wt % with a melting enthalpy of 96.8 J/g for the EPDM + RT28 + ENV sample. TGA tests highlighted the influence of paraffin in decreasing the thermal stability of the produced samples at high temperature but not in the working range of buildings materials. Shore A hardness and compression tests highlighted the dependency of the mechanical behaviour of the produced materials on the temperature, due to the presence of paraffin that acted as a softener at the molten state and as a hardener when crystallized. The thermal conductivity of EPDM + RT28 + ENV panels (around 0.15 W/m·K) is slightly higher with respect to that of the EPDM reference panel (0.11 W/m·K) and it is not influenced by the testing temperature. Measurements of the TES performances were carried out through heating/cooling tests of testing boxes insulated with an internal panel of EPDM + RT28 + ENV. These tests, carried out in a temperature interval from 16 to 31 °C, (typical summer conditions in Trento, Italy) revealed that the TES-panels were able to keep the internal temperature of the box always lower than 27 °C and that the time required to reach an internal temperature of 26 °C was one hour longer with respect to that of a wood box insulated with the reference EPDM panel. Similar results were observed 15 months later, evidencing the stability of the assembled testing box.

Considering the cost of the raw materials according to quotations available to the authors (EPDM compound 4.0 €/kg, NBR envelope 3.7 €/kg, RT28HC 16.0 €/kg, Cloisite 17.5 €/kg), it is possible to evaluate a cost of around 10.4 €/kg for the EPDM + RT28 + ENV sample. Comparing this panel with a commercial product produced by Rubitherm GmbH and consisting of a PCM in an aluminium case, it is possible to highlight some advantages and disadvantages of the two products. The commercial product is characterized by a higher thermal energy storage capacity (240 J/g) and by an easier production method; on the other hand its rigid structure may limit the application when curved surfaces should be insulated. Conversely, the panel produced in this work can be applied also to non-uniform and curved surfaces, even for floor application. In case of impact, the composition of the material would affect the system behaviour, i.e. permanent deformation of the aluminium panel, and recovery of the rubber panel. However an evident disadvantage and limit of this elastomeric panel is the fire stability and the possible leakage after long storage; on the contrary, an advantage seems to be the higher thermal inertia due to the lower thermal conductivity of rubber with respect to aluminium. An economical comparison considering both production and material costs would be useful in order to classify them.

In conclusion, these modified EPDM/NBR panels with paraffin clearly evidenced promising properties (no leakage and residual TES capacity of 97 J/g, corresponding to 504 kJ/m^2) in building applications and, using PCMs with different melting points, also for the thermal management of refrigerated trucks. Further research will be devoted to simulations at a larger scale, to the evaluation of the long-term performances, to the evaluation of the impact on environment, human health and ecosystem and to the study of their fire behaviour.

Declaration of Competing Interest

The authors declare that they have no known competing financial interests or personal relationships that could have appeared to influence the work reported in this paper.

Acknowledgements

This work was partially funded by Provincia Autonoma di Trento (Italy) through Legge 6/99, project “Compositi elastomerici a transizione di fase [E-PCM] prat. n. 23-16”.

References

[1] A. GhaffarianHoseini, N.D. Dahlan, U. Berardi, A. GhaffarianHoseini, N. Makaremi, M. GhaffarianHoseini, Sustainable energy performances of green buildings: A review of current theories, implementations and challenges, Renewable and Sustainable Energy Reviews 25 (2013) 1–17.
[2] S. VijayaVenkataRaman, S. Iniyan, R. Goic, A review of climate change, mitigation and adaptation, Renewable and Sustainable Energy Reviews 16 (1) (2012) 878–897.
[3] H. Ritchie, M. Roser, *Energy*. Our world in Data (2020).

[4] O. Schwedes, The Field of Transport Policy: An Initial Approach, German Policy Studies 7 (2) (2011) 7–41.
[5] International energy agency, *European Union 2020. Energy policy review*. 2020.
[6] V. Moutinho, M. Madaleno, R. Inglesi-Lotz, E. Dogan, Factors affecting CO2 emissions in top countries on renewable energies: A LMDI decomposition application, Renewable and Sustainable Energy Reviews 90 (2018) 605–622.
[7] European environmental agency, *Total greenhouse gas emission trends and projections in Europe*. 2019.
[8] European commission, *Results of the EUCO3232.5 scenario on Member States*. 2019.
[9] European environmental agency, *Energy efficiency in transformation*. 2009.
[10] P. Meshgin, Y. Xi, Y. Li, Utilization of phase change materials and rubber particles to improve thermal and mechanical properties of mortar, Construction and Building Materials 28 (1) (2012) 713–721.
[11] B. He, V. Martin, F. Setterwall, Phase transition temperature ranges and storage density of paraffin wax phase change materials, Energy 29 (11) (2004) 1785–1804.
[12] M.R. Anisur, M.H. Mahfuz, M.A. Kibria, R. Saidur, I.H.S.C. Metselaar, T.M. I. Mahlia, Curbing global warming with phase change materials for energy storage, Renewable and Sustainable Energy Reviews 18 (2013) 23–30.
[13] D. Fernandes, F. Pitié, G. Cáceres, J. Baeyens, Thermal energy storage: "How previous findings determine current research priorities", Energy 39 (1) (2012) 246–257.
[14] G. Li, X. Zheng, Thermal energy storage system integration forms for a sustainable future, Renewable and Sustainable Energy Reviews 62 (2016) 736–757.
[15] M. Mofijur, T. Mahlia, A. Silitonga, H. Ong, M. Silakhori, M. Hasan, N. Putra, S. M. Rahman, Phase Change Materials (PCM) for Solar Energy Usages and Storage: An Overview, Energies 12 (16) (2019) 3167, https://doi.org/10.3390/en12163167.
[16] A.L. Facci, V.K. Krastev, G. Falcucci, S. Ubertini, Smart integration of photovoltaic production, heat pump and thermal energy storage in residential applications, Solar Energy 192 (2019) 133–143.
[17] Sunamp Ltd, *UniQ eHW Heat Battery Installation and User Manual*. 2020.
[18] H. Bo, E.M. Gustafsson, F. Setterwall, Phase transition temperature ranges and storage density of paraffin wax phase change materials, Energy 24 (12) (1999) 1015–1028.
[19] S. Peng, A. Fuchs, R.A. Wirtz, Polymeric phase change composites for thermal energy storage, Journal of Applied Polymer Science 93 (3) (2004) 1240–1251.
[20] A.M. Borreguero, M. Carmona, M.L. Sanchez, J.L. Valverde, J.F. Rodriguez, Improvement of the thermal behaviour of gypsum blocks by the incorporation of microcapsules containing PCMS obtained by suspension polymerization with an optimal core/coating mass ratio, Applied Thermal Engineering 30 (10) (2010) 1164–1169.
[21] A. Dorigato, M.V. Ciampolillo, A. Cataldi, M. Bersani, A. Pegoretti, Polyethylene wax/EPDM blends as shape-stabilized phase change materials for thermal energy storage, Rubber Chemistry and Technology 90 (3) (2017) 575–584.
[22] G. Song, S. Ma, G. Tang, Z. Yin, X. Wang, Preparation and characterization of flame retardant form-stable phase change materials composed by EPDM, paraffin and nano magnesium hydroxide, Energy 35 (5) (2010) 2179–2183.
[23] C. Alkan, K. Kaya, A. Sari, Preparation, Thermal Properties and Thermal Reliability of Form-Stable Paraffin/Polypropylene Composite for Thermal Energy Storage | SpringerLink, Journal of polymer and the environment 17 (2009) 254.
[24] W.-L. Cheng, R.-M. Zhang, K. Xie, N.a. Liu, J. Wang, Heat conduction enhanced shape-stabilized paraffin/HDPE composite PCMs by graphite addition: Preparation and thermal properties, Solar energy materials and solar cells 94 (10) (2010) 1636–1642.
[25] H. Inaba, P. Tu, Evaluation of thermophysical characteristics on shape-stabilized paraffin as a solid-liquid phase change material, Heat and mass transfer 32 (4) (1997) 307–312.
[26] K. Kaygusuz, A. Sari, High Density Polyethylene/Paraffin Composites as Form-stable Phase Change Material for Thermal Energy Storage, Energy Sources, Part A: Recovery, Utilization, and Environmental Effects 29 (3) (2007) 261–270.
[27] K. Kaygusuz, C. Alkan, A. Sari, O. Uzun, Encapsulated Fatty Acids in an Acrylic Resin as Shape-stabilized Phase Change Materials for Latent Heat Thermal Energy Storage, Energy Sources, Part A: Recovery, Utilization, and Environmental Effects 30 (11) (2008) 1050–1059.
[28] W. Mhike, W.W. Focke, J.P.L. Mofokeng, A.S., Thermally conductive phase-change materials for energy storage based on low-density polyethylene, soft Fischer-Tropsch wax and graphite, Thermochimica Acta 572 (2012) 75–82.
[29] M. Xiao, B. Feng, K. Gong, Preparation and performance of shape stabilized phase change thermal storage materials with high thermal conductivity, Energy conversion and management 43 (1) (2002) 103–108.
[30] Y. Hong, G. Xin-shi, Preparation of polyethylene–paraffin compound as a form-stable solid-liquid phase change material, Solar energy materials and solar cells 64 (1) (2000) 37–44.
[31] I. Krupa, G. Miková, A.S. Luyt, Polypropylene as a potential matrix for the creation of shape stabilized phase change materials, European polymer journal 43 (3) (2007) 895–907.
[32] A. Sari, C. Alkan, A. Karaipekli, O. Uzun, Poly(ethylene glycol)/poly(methyl methacrylate) blends as novel form-stable phase-change materials for thermal energy storage, Journal of applied polymer science 116 (2) (2009) 929–933.
[33] Q. Cao, P. Liu, Hyperbranched polyurethane as novel solid–solid phase change material for thermal energy storage, European polymer journal 42 (11) (2006) 2931–2939.
[34] F. Valentini, A. Dorigato, A. Pegoretti, M. Tomasi, G.D. Sorarù, M. Biesuz, Si3N4 nanofelts/paraffin composites as novel thermal energy storage architecture, Journal of Materials Science 56 (2) (2021) 1537–1550.
[35] C. Castellón, M. Medrano, J. Roca, L.F. Cabeza, M.E. Navarro, A.I. Fernández, A. Lázaro, B. Zalba, Effect of microencapsulated phase change material in sandwich panels, Renewable Energy 35 (10) (2010) 2370–2374.
[36] F. Galvagnini, A. Dorigato, F. Valentini, V. Fiore, M. La Gennusa, A. Pegoretti, Multifunctional polyurethane foams with thermal energy storage/release capability, Journal of Thermal Analysis and Calorimetry 147 (1) (2022) 297–313.
[37] F. Valentini, L. Fambri, A. Dorigato, A. Pegoretti, et al., Production and Characterization of TES-EPDM Foams With Paraffin for Thermal Management Applications, Frontiers in Materials 8 (2021) 101.
[38] F. Valentini, A. Dorigato, A. Pegoretti, Novel EPDM/paraffin foams for thermal energy storage applications, Rubber Chemistry and Technology 94 (3) (2021) 432–448.
[39] L.F. Cabeza, A. Castell, C. Barreneche, A. de Gracia, A.I. Fernández, Materials used as PCM in thermal energy storage in buildings: A review, Renewable and Sustainable Energy Reviews 15 (3) (2011) 1675–1695.
[40] A.M. Borreguero, I. Garrido, J.L. Valverde, J.F. Rodríguez, M. Carmona, Development of smart gypsum composites by incorporating thermoregulating microcapsules, Energy and Buildings 76 (2014) 631–639.
[41] T. Khadiran, M.Z. Hussein, Z. Zainal, R. Rusli, Advanced energy storage materials for building applications and their thermal performance characterization: A review, Renewable and Sustainable Energy Reviews 57 (2016) 916–928.
[42] A. Sharma, V.V. Tyagi, C.R. Chen, D. Buddhi, Review on thermal energy storage with phase change materials and applications, Renewable and Sustainable Energy Reviews 13 (2) (2009) 318–345.
[43] D. Rigotti, A. Dorigato, A. Pegoretti, 3D printable thermoplastic polyurethane blends with thermal energy storage/release capabilities, Materials Today Communications 15 (2018) 228–235.
[44] E. Fallahi, M. Barmar, M.H. Kish, Preparation of Phase-change Material Microcapsules with Paraffin or Camel Fat Cores: Application to Fabrics, Iranian Polymer Journal 19 (4) (2010) 277–286.
[45] F. Salaün, E. Devaux, S. Bourbigot, P. Rumeau, Thermoregulating response of cotton fabric containing microencapsulated phase change materials, Thermochimica acta 506 (2010) 82–93.
[46] G. Fredi, A. Dorigato, A. Pegoretti, *Multifunctional glass fiber/polyamide composites with thermal energy storage/release capability*. eXPRESS, Polymer Letters 12 (4) (2018) 349–364.
[47] S. Datta, Synthetic elastomers, in: J.R. White, S.K. De (Eds.), Rubber technologist's handbook, Rapra technology ltd., Shawbury, UK, 2001, pp. 61–64.
[48] M.G. Mohamed, S.L. Abd-El-Messieh, S. El-Sabbagh, A.F. Younan, Electrical and mechanical properties of polyethylene–rubber blends, Journal of Applied Polymer Science 69 (4) (1998) 775–783.
[49] D.E. El-Nashar, G. Turky, Effect of Mixing Conditions and Chemical Cross-Linking Agents on the Physicomechanical and Electrical Properties of NR/NBR Blends, Polymer-Plastics Technology and Engineering 42 (2) (2003) 269–284.
[50] V. Jovanović, S. Samaržija-Jovanović, J. Budinski-Simendić, G. Marković, M. Marinović-Cincović, Composites based on carbon black reinforced NBR/EPDM rubber blends, Composites Part B: Engineering 45 (1) (2013) 333–340.
[51] C. Albano, M.N. Ichazo, I. Boyer, M. Hernández, J. González, A. Karam, M. Covis, Study of the thermal stability of Nitrile rubber-coconut flour compounds, Polymer Degradation and Stability 97 (11) (2012) 2202–2211.
[52] P.R. Morrell, M. Patel, A.R. Skinner, Accelerated thermal ageing studies on nitrile rubber O-rings, Polymer Testing 22 (6) (2003) 651–656.
[53] Y. Chen, S. Gao, C. Liu, Y. Situ, J. Liu, H. Huang, Preparation of PE-EPDM based phase change materials with great mechanical property, thermal conductivity and photo-thermal performance, Solar Energy Materials and Solar Cells 200 (2019) 109988, https://doi.org/10.1016/j.solmat.2019.109988.
[54] Ribeiro de Souza, D.A., *Private communication*. Private communication.
[55] Rubitherm. *Datasheet RT28HC*. 2021 21/02/2021]; Available from: https://www.rubitherm.eu/media/products/datasheets/Techdata_- RT28HC_EN_09102020.PDF.
[56] H. Weingrill, W. Hohenauer, K. Resch-Fauster, C. Zauner, Analyzing Thermal Conductivity of Polyethylene-Based Compounds Filled with Copper, Macromolecular Materials and Engineering 304 (4) (2019) 1800644, https://doi.org/10.1002/mame.v304.410.1002/mame.201800644.
[57] W.N. dos Santos, Thermal properties of polymers by non-steady-state techniques, Polymer Testing 26 (4) (2007) 556–566.
[58] A. Kasaeian, L. Bahrami, F. Pourfayaz, E. Khodabandeh, W.M. Yan, Experimental studies on the applications of PCMs and nano-PCMs in buildings: A critical review, Energy Building 154 (2017) 96–112.
[59] X. Kong, C. Yao, P. Jie, Y. Liu, C. Qi, X. Rong, Development and thermal performance of an expanded perlite-based phase change material wallboard for passive cooling in building, Energy Buildings 152 (2017) 547–557.
[60] C. Yao, X. Kong, Y. Li, Y. Du, C. Qi, Numerical and experimental research of cold storage for a novel expanded perlite-based shape-stabilized phase change material wallboard used in building, Energy Conversion Management 155 (2018) 20–31.
[61] K.O. Lee, M.A. Medina, X. Sun, X. Jin, Thermal performance of phase change materials (PCM)-enhanced cellulose insulation in passive solar residential building walls, Solar Energy 163 (2018) 113–121.
[62] A.G. Entrop, H.J.H. Brouwers, A.H.M.E. Reinders, Experimental research on the use of micro encapsulated Phase Change Materials to store solar energy in concrete floors and to save energy in Dutch houses, Solar Energy 85 (5) (2011) 1007–1020.
[63] L.F. Cabeza, C. Castellón, M. Nogués, M. Medrano, R. Leppers, O. Zubillaga, Use of microencapsulated PCM in concrete walls for energy savings, Energy Buildings 39 (2) (2007) 113–119.
[64] R. Barzin, J.J.J. Chen, B.R. Young, M.M. Farid, Application of PCM underfloor heating in combination with PCM wallboards for space heating using price-based control system, Applied Energy 148 (2015) 39–48.

[65] R. Gulfram, P. Zhang, Z. Meng, Advanced thermal systems driven by paraffin-based phase change materials – A review, Applied Energy 238 (2019) 582–611.
[66] R. Daghigh, A. Shafieian, Energy and exergy evaluation of an integrated solar heat pipe wall system for space heating, Sädhanä 41 (2016) 877–886.
[67] D. Ling, G. Mo, Q. Jiao, J. Wei, X. Wang, *Research on solar heating system with phase change thermal energy storage*, Energy Procedia 91 (2016) 415–420.
[68] Y. Zhang, C. Chen, H. Jiao, W. Wang, Z. Shao, D. Qi, R. Wang, *Thermal performance of new hybrid solar energy-phase change storage-floor radiant heating system*, Procedia Engineering 146 (2016) 89–99.
[69] A. Koca, H.F. Oztop, T. Koyun, Y. Varol, Energy and exergy analysis of a latent heat storage system with phase change material for a solar collector, Renewable Energy 33 (2008) 567–574.
[70] C. Arkar, T. Suklje, B. Vidrih, S. Medved, Performance analysis of a solar air heating system with latent heat storage in a lightweight building, Applied Thermal Engineering 95 (2016) 281–287.
[71] Z. Zhao, M.T. Arif, A.M. Oo, Solar thermal energy with molten-salt storage for residential heating application, Energy Procedia 110 (2017) 243–249.
[72] A. Hasan, H. Alnoman, Y. Rashid, Impact of integrated photovoltaic-phase change material system on building energy efficiency in hot climate, Energy Buildings 130 (2016) 495–505.
[73] G. Gan, Y. Xiang, Experimental investigation of a photovoltaic thermal collector with energy storage for power generation, building heating and natural ventilation, Renewable Energy 150 (2020) 12–22.
[74] M.O. Lari, A.Z. Sahin, Effect of retrofitting a silver/water nanofluid-based photovoltaic/thermal (PV/T) system with a PCM-thermal battery for residential applications, Renewable Energy 122 (2018) 98–107.
[75] W. Lin, Z. Ma, P. Cooper, M.I. Sohel, L. Yang, Thermal performance investigation and optimization of buildings with integrated phase change materials and solar photovoltaic thermal collectors, Energy Buildings 116 (2016) 562–573.
[76] S.R.L. da Cuhna, J.L.B. de Aguiar, Phase change materials and energy efficiency of buildings: A review of knowledge, J Energy Storage 127 (2020), 101083.
[77] J.L. Reyez-Araiza, et al., Thermal Energy Storage by the Encapsulation of Phase Change Materials in Building Elements—A Review, Materials. 14 (2021) 1420.
[78] H. Selvnes, Y. Allouche, R.I. Manescu, A. Hafner, Review on cold thermal energy storage applied to refrigeration systems using phase change materials, Thermal Science and Engineering Progress. 22 (2021), 100807.